AIMS Materials Science, 9 (5): 770–784.
DOI: 10.3934/matersci.2022047
Received: 23 June 2022
Revised: 03 September 2022
Accepted: 08 September 2022
Published: 30 September 2022

http://www.aimspress.com/journal/Materials

Research article

Effect of monobasic/dibasic phosphate salts on the crystallinity, physical properties and photocatalytic performance of Ag_3PO_4 material

Hung Nguyen Manh[1,3], Oanh Le Thi Mai[1,2,*], Chung Pham Do[2], Mai Vu Thanh[1,4], Anh Nguyen Thi Diep[2], Dao La Bich[2], Hang Lam Thi[1,5], Duyen Pham Thi[6] and Minh Nguyen Van[1,2]

[1] Center for Nano Science and Technology, Hanoi National University of Education, 136 Xuan Thuy Road, Cau Giay District, Hanoi 100000, Vietnam
[2] Department of Physics, Hanoi National University of Education, 136 Xuan Thuy Road, Cau Giay District, Hanoi 100000, Vietnam
[3] Hanoi University of Mining and Geology, Duc Thang ward, North Tu Liem District, Hanoi 100000, Vietnam
[4] Institute of Materials Science, Vietnam Academy of Science and Technology, 18 Hoang Quoc Viet, Hanoi 100000, Viet Nam
[5] Faculty of Basic Sciences, Hanoi University for Natural Resources and Environment, 41A Phu Dien Road, North Tu Liem, Hanoi 100000, Vietnam
[6] Faculty of Basic Sciences, Military Science Academy, Le Trong Tan, Dinh Cong, Hoang Mai, Hanoi 100000, Vietnam

* **Correspondence:** Email: lemaioanh@gmail.com.

Abstract: Ag_3PO_4 was prepared by the precipitation method using monobasic/dibasic phosphate salts (K_2HPO_4, KH_2PO_4, Na_2HPO_4, NaH_2PO_4) as a precipitating agent. The environment created by the precursor salts strong affected on the crystallinity and the morphology of Ag_3PO_4. Ag_3PO_4 synthesized from dibasic phosphate salts exhibited pseudospherical morphology and small particle size while monobasic phosphate salts promoted crystallization, resulting in a large grain size and a very diverse grain morphology. Ag_3PO_4 prepared from dibasic phosphate salts (K_2HPO_4 and

Na_2HPO_4) exhibited superior photocatalytic ability, completely degrading rhodamine B (RhB) in 8 min and 10 min under Xenon lamp irradiation, respectively. This result once again confirms the necessity of particle size reduction in the production of photocatalysts.

Keywords: photocatalytic; dibasic phosphate salt; monobasic phosphate salt; crystallinity

1. Introduction

In the past decades, in the face of water pollution caused by organic dyes from various industrial plants such as paper, printing ink, fabic and industrial dyeing, etc., the search for solutions to improve the water environment is the main concern of researchers. With the achievements of science and technology, water pollution treatment through advanced oxidation process AOP using semiconductor photocatalysts was born and developed strongly [1–3]. Photocatalysis is a method that exhibits outstanding advantages compared to conventional methods such as high efficiency, low cost, environmental friendliness. In addition, it can also take advantage of the infinite excitation energy from the Sun. Since Fujishima and Honda first discovered the photocatalytic ability of TiO_2 electrode in 1972 [4], metal oxide-based photocatalysts such as TiO_2, ZnO, SnO_2, ABO_4, $A_2B_2O_7$, etc. have been studied extensively and shown high photocatalytic efficiency. However, a major drawback of these semiconductors is the large energy band gap (>3 eV), which can only use ultraviolet light, a small fraction of solar radiation, to stimulate electron-hole generation. A large part of research effort on these materials is focused on modifying materials to have smaller band gap such as doping [5–7], compositing [8–11] and loading [12,13]. At the same time, the search and development of new photocatalysts that work efficiently under visible light has always been a big goal in recent years.

Among the new materials discovered in the last decade, Ag_3PO_4 (APO) is considered as one of the bright candidates for visible light photocatalyst [14]. It is proven that APO has a narrow band gap energy of 2.43 eV and an excellent photocatalytic activity with a quantum yield of 90% [15] with the ability to decompose a wide range of organic substances such as rhodamine B [16], bisphenol A [17], phenol [18,19], methylene blue [20], quinoline yellow [21], methyl orange [22], and microcystins [23], etc. Studies show that the morphology and particle size of APO greatly affect the photocatalytic performance of the material. In turn, APO particle morphology is influenced by several factors such as the method of synthesis (co-precipitation, hydrothermal, microwave-assisted chemistry, etc.), phosphate ion source (basic phosphate salts or phosphoric acid), the pH of the starting solution and surfactant. For example, APO particles with very different pseudospherical particle morphology and size were prepared from basic phosphate salts Na_3PO_4, Na_2HPO_4, NaH_2PO_4 by co-precipitation method in which the sample prepared from Na_2HPO_4 exhibited the highest photocatalytic efficiency to degrade methylene blue [24]. Meanwhile, tetrahedral APO particles were produced using phosphoric acid H_3PO_4 [24]. Visible light-responsive Ag_3PO_4 photocatalysts with fern-like, multipod-like and tetrapod-like morphologies were successfully synthesized by facile soft-chemical technique from phosphoric acid H_3PO_4 and $AgNO_3$ in the presence of tetrahydrofuran (THF)

surfactant with a THF/water volumetric ratio of 0:1, 0.11:1, 0.13:1 [25]. By decreasing pH through increasing ammonia NH_4 concentration at 0.00 M, 0.05 M, 0.15 M and 0.30 M, APO particles of decreasing size with NH_4 concentration are produced and accordingly photocatalytic ability increased [26]. Extremely small APO nanoparticles of about 10 nm with outstanding visible light photocatalysis were produced by simple ion-exchange method from $(NH_4)_2HPO_4$ [27]. APO composed of several microcrystals with polydisperse size and shape were synthesized by microwave-assisted hydrothermal method using $(NH_4)_2HPO_4$ as phosphate ion source [28]. Different concentrations of KH_2PO_4 initiator were also used to change the morphology and size of APO particles and thus control its photocatalytic ability [15]. In general, the studies used phosphate moiety as the precipitation agent in the form of salts or acids. However, to date, there have been no studies specifically comparing the effect of different phosphate moieties on the structure and physical and photocatalytic properties of APO.

In this study, we would like to clarify the influence of phosphate sources as monobasic and dibasic salts on the morphology and photocatalytic properties of APO. The selected phosphate salts are of two metals potasium and sodium (K_2HPO_4, KH_2PO_4, Na_2HPO_4, NaH_2PO_4). The work focused on showing which phosphate source (monobasic or dibasic) is more suitable to produce APO with strong photocatalytic activity. In addition, the structural and other physical properties were also thoroughly analyzed to support the interpretation of the photocatalytic activity.

2. Materials and methods

2.1. Materials

Silver nitrate ($AgNO_3$, Merck, 99%), potassium phosphate dibasic trihydrate ($K_2HPO_4.3H_2O$, Merck, 99%), potassium phosphate monobasic (KH_2PO_4, Merck, 99%), sodium phosphate dibasic dodecahydrate ($Na_2HPO_4{\cdot}12H_2O$, Merck, 99%), and sodium phosphate monobasic dihydrate ($NaH_2PO_4{\cdot}2H_2O$, Merck, 99%) were used as starting chemicals. Rhodamine B ($C_{28}H_{31}ClN_2O_3$, Merck, 95%) was used as an organic colorant in the photocatalytic test. These starting materials were used without further purification. A Xenon lamp (300W/220V) with an ultraviolet filter were used as the visible light source irradiation.

2.2. Synthesis of photocatalysts

In this study, we synthesize Ag_3PO_4 photocatalyst by a simple precipitation method. An amount of $AgNO_3$ was dissolved in a beaker containing 150 mL of distilled water to obtain an Ag^+ 0.02 M solution. In another beaker, a suitable phosphate salt (K_2HPO_4, KH_2PO_4, Na_2HPO_4, NaH_2PO_4) is dissolved in an analysis amount of distilled water such that a 0.02 M solution of PO_4^{3-} is obtained. The stoichiometric amount of phosphate salts was specified such that the Ag^+/PO_4^- ratio is of 3:1.5 according to our previous investigation for optimization of synthesis condition. The solution containing Ag^+ ions was then slowly added into the solution containing PO_4^{3-} ions and magnetically stirred to obtain a homogeneous solution. This solution was continued to be magnetically stirred for the next 3 h at room temperature until a stable amount of yellow precipitate was formed. The

precipitate was filtered and washed 5 times with distilled water before being dried at 100°C to obtain a yellow powder of Ag_3PO_4.

Samples of APO prepared from different salts K_2HPO_4, KH_2PO_4, Na_2HPO_4, and NaH_2PO_4 were respectively named after the chemical formula of the starting salt as APOK2H, APOKH2, APONa2H, and APONaH2 for convenience in description.

2.3. Characterization

X-ray diffractometer (XRD, Brucker D8 Advance) using Cu Kα radiation (λ = 1.54064 Å) was used to determine the crystal structure of as-synthesized APO samples with Bragg angles ranging from 10º to 110º. The surface morphology of the samples was observed using a scanning electron microscope (SEM, JED-2300). The Brunauer-Emmett-Teller (BET) surface area was analyzed using a high-performance adsorption analyzer (Micromeritics 3Flex). An infrared spectrophotometer (Shimadzu IR Prestige-21) was used to measure the Fourier transform infrared (FTIR) absorption spectra. A Raman spectrophotometer (Horiba LabRam HR Evolution) using a 532 nm laser beam as the excitation source was used to measure Raman scattering spectra. UV-vis diffuse reflectance spectra (DRS) were performed on a UV-vis spectrophotometer (Jasco V670). Luminescence (PL) spectra were carried out on a fluorescence spectrometer (Nanolog Horiba iHR 550) using an excitation beam at 350 nm.

2.4. Photocatalytic activity test

In this study, visible-light photocatalytic activity of Ag_3PO_4 was evaluated based on the degradation of 10 ppm rhodamine B (RhB) solution. The visible light used for excitation is obtained from a Xenon lamp (300 W/220 V) using an ultraviolet filter.

At the first step, 30 mL of 20 ppm RhB solution was placed in a 6 cm diameter beaker. In another beaker, 0.6 g of APO was dissolved in 30 ml of distilled water, sonicated for 30 min. Next, slowly add the 20 ppm RhB solution into the APO-contained beaker to obtain a mixture with RhB concentration of 10 ppm. The mixture was immediately magnetically stirred in a dark chamber for 30 min to reach adsorption-desorption equilibrium. After the first 10 min of dark stirring, 4 mL of the solution was removed to evaluate the adsorption capacity of the sample. After dark stirring for 30 min, the solution was illuminated under a Xenon lamp using a UV-cut filter. The distance between the Xenon lamp and the surface of the RhB solution is around 10 cm (~23000 lux illuminance). An amount of 4 mL of solution was removed every one min and centrifuged at 4000 rpm to remove the APO powder. Absorption spectra were used to evaluate the remaining RhB concentration in solution (using 554 nm characteristic absorption peak of RhB).

3. Results and discussion

Figure 1a shows the X-ray diffraction patterns of as-synthesized Ag_3PO_4 (APO) photocatalysts with different starting phosphate salts (K_2HPO_4, KH_2PO_4, Na_2HPO_4, NaH_2PO_4). All the patterns match well with the body-centered cubic Ag_3PO_4 according to JCPDS card No. 06-0505 without any

strange reflexes of the impurity phases. A comparison of the (210) plane position was carried out (Figure 1b) that indicates a given shift to the larger 2-theta angle when using monobasic phosphate salts (APOKH2, APONaH2), which should theoretically lead to a smaller lattice parameter a. Table 1 presents calculated lattice constant a as well as unit cell volume V in angstrom unit, in which the lattice constants a is 5.962 Å, 5.945 Å, 5.965 Å, and 5.942 Å for the APOK2H, APOKH2, APONa2H, and APONaH2 samples, respectively. Obviously, the crystals prepared from the monobasic phosphate salts possess the smaller lattice parameter than that of the samples synthesized from dibasic salt. A comparation of the intensity of the line (210) showed greater intensity for the samples fabricated from the monobasic phosphate salts where the ratios of I_{APOKH2}/I_{APOK2H} and $I_{APONaH2}/I_{APONa2H}$ are 1.05 and 1.50, respectively. In addition, the crystallinity is also evaluated by the crystallite size D_{XRD} that can be inferred from the full width at half maximum $FWHM$ of diffraction lines using the Debye-Scherrer equation. Figure 1b shows the narrower of the (210) line for the samples APOKH2 and APONaH2, leading to the calculated results for a larger D_{XRD} as shown in Table 1. The crystallite size is 41 nm, 48 nm, 33 nm, and 48 nm for the APOK2H, APOKH2, APONa2H, and APONaH2 samples, respectively. The expression of the small lattice parameter and the large crystal size shows that the samples APOKH2 and APONaH2 samples crystallize better than those synthesized from dibasic phosphate salts. This may be a manifestation of the influence of the pH on the crystallization of APO, the lower the pH, the greater the crystallinity. The strong crystallization of APO synthesized from monobasic phosphate salts could be explained by the competition between OH^- and PO_4^{3-} that reacts with Ag on the surface of Ag_3PO_4 nuclei during the growth proccess [29]. As well known, KH_2PO_4 and NaH_2PO_4 are acidic salts (pH ~ 5.7) while K_2HPO_4 and Na_2HPO_4 are basic salts (pH ~ 7.5). In the solvent of monobassic phosphate salt, the amount of OH^- ions on the surface of the Ag_3PO_4 nucleus is less than in the solvent of dibasic phosphate salts, so PO_4^{3-} easily combines with Ag^+ leading to better growth of APOKH2 and APONaH2 crystals.

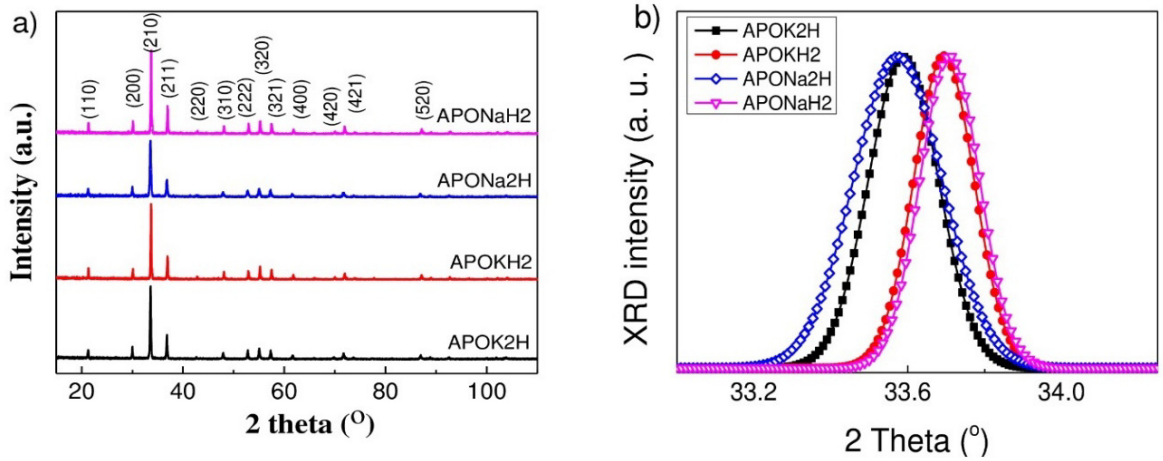

Figure 1. (a) XRD patterns of Ag_3PO_4 photocatalysts synthesized from different phosphate salts (K_2HPO_4, KH_2PO_4, Na_2HPO_4, NaH_2PO_4) and (b) a comparison of (201) reflexes position in different samples.

Table 1. Some parameters of Ag_3PO_4 crystals synthesized from different phosphate salts (K_2HPO_4, KH_2PO_4, Na_2HPO_4, NaH_2PO_4) such as lattice constant a, unit cell volume V, full width of half maximum $FWHM$, crystal size D_{XRD} and particle size D_{SEM}.

Samples	APOK2H	APOKH2	APONa2H	APONaH2
$a = b = c$ (Å)	5.962	5.945	5.965	5.942
V (Å^3)	212.022	210.128	212.207	209.830
$FWHM$ (°)	0.214	0.185	0.272	0.182
Crystallite size D_{XRD} (nm)	41	48	32	48
Particle size D_{SEM} (μm)	0.8	3.2	0.4	1.6

The surface morphology of as-synthesized AOP particles was investigated by the SEM measurements (Figure 2). Particle size distributions were performed through ImageJ software and is represented in Figure 3. Figure 2a,c represent the external morphology of the APOK2H and APONa2H samples, consisting of pseudospherical particles of averaging diameter around of 800 nm and 400 nm (Figure 3a,c), respectively, with occasional inclusions of a few particles with geometric polygon faces (dotted circle). This result complements the inference that the OH^- group inhibits the reaction of PO_4^{3-} and Ag^+ to form Ag_3PO_4 in basic solvents. Therefore, not only the crystal grain size is small, but there is also no preferred crystal growth orientation. Meanwhile, the SEM images of the two samples APOKH2 and APONaH2 (Figure 2b,d) show much larger particles, averaging around 3.2 μm and 2.6 μm, respectively. In addition, most particles have a polygonal shape with distinct geometrical facets. The sample APOKH2 contains mainly dodecahedral particles while the sample APONaH2 contains cubic ones. In the APOKH2 sample, a variety of grain morphology can also be found such as tetrapot (i), pyramid (ii), and triangular plate (iii) (inset figure in Figure 2b). Therefore, it can be said that low pH conditions not only facilitated stronger growth of APO crystallites but also promote anisotropic crystallization along certain prority axes to produce crystals with diverse morphologies and sizes many times larger than those of APO prepared from high pH solvent [15,29,30]. In addition, correlation between crystal size D_{XRD} and particle size D_{SEM} (Table 1) also shows that low pH conditions both promote crystallization and agglomeration of single crystals into large particles.

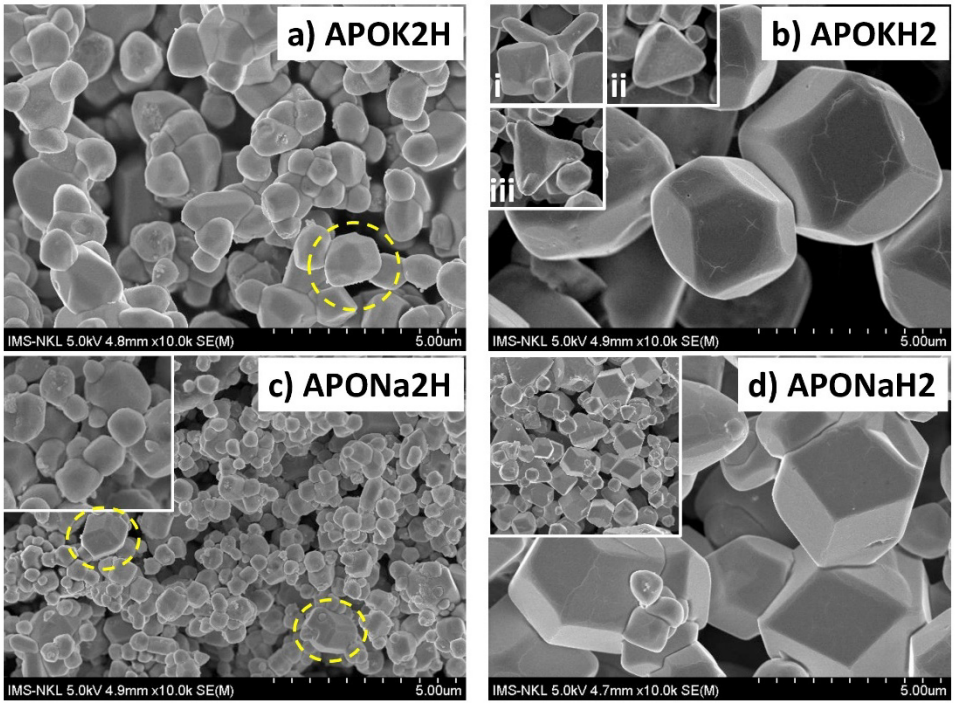

Figurre 2. SEM images of Ag_3PO_4 photocatalysts synthesized from different phosphate salts (a) K_2HPO_4, (b) KH_2PO_4, (c) Na_2HPO_4, and (d) NaH_2PO_4.

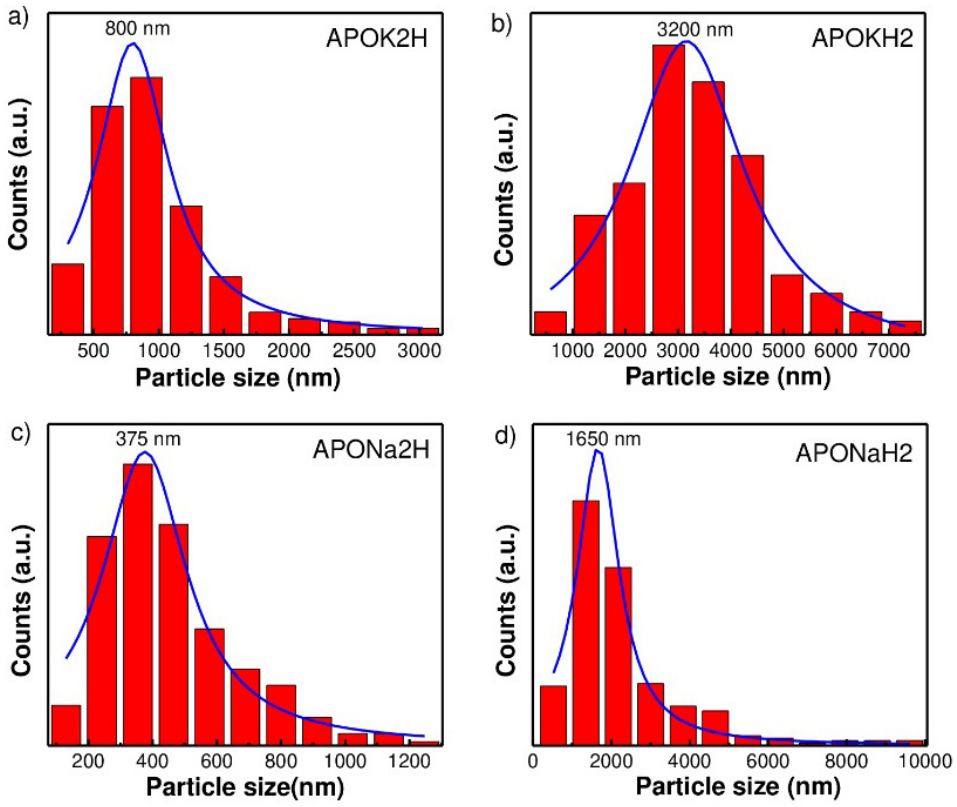

Figure 3. Particle size distribution of Ag_3PO_4 photocatalysts synthesized from different phosphate salts (a) K_2HPO_4, (b) KH_2PO_4, (c) Na_2HPO_4, and (d) NaH_2PO_4.

Figure 4a shows the FTIR absorption spectra of as-synthesized APO samples which indicates some sharp absorbance centered at 546 cm^{-1}, 1018 cm^{-1}, 1385 cm^{-1}, 1661 cm^{-1}, 2364 cm^{-1}, and 3234 cm^{-1}. The peaks at 546 cm^{-1} and 1018 cm^{-1} are attributed to the characteristic vibrations of the $[PO_4]$ cluster in crystal lattice, corresponding to $\nu 4$ antisymmetric bending mode and $\nu 3$ antisymmetric stretching mode [31,32]. Two peaks at 1661 cm^{-1} and 3234 cm^{-1} could be attributed to the oscillations of water molecules adsorbed on the APO surface while the adsorbed CO_2 molecules exhibited vibration peak at the 2364 cm^{-1} [33]. Alternatively, the band at 1390 cm^{-1} can be specified for nitrate groups generated from synthetic residues. To indirectly observe the change in APO lattice structure, a detailed comparison of the FTIR absorption between 400–1200 cm^{-1} was carried out and presented in Figure 4b. The results show that while the three APOK2H, APONa2H, and APOKH2 samples exhibit relatively similar FTIR absorption peaks of the $[PO_4]$ group at 546 cm^{-1}, 1004 cm^{-1} and 1037 cm^{-1}, the APONaH2 sample shows a shift of peaks towards a larger frequency, which is consistent with the smallest lattice constant of APONaH2 as observed in the XRD results.

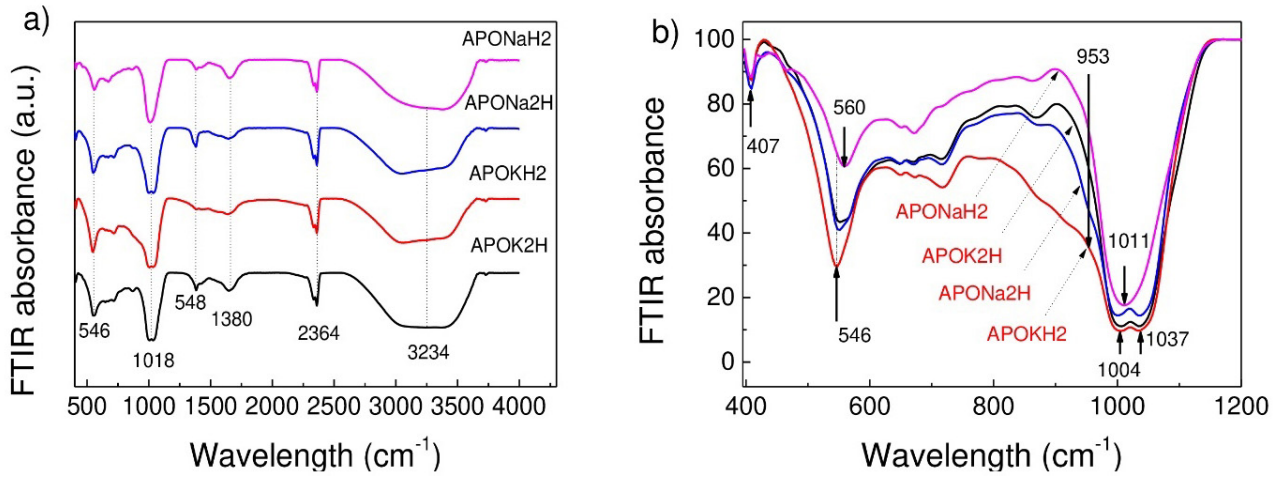

Figure 4. (a) FTIR spectra of Ag_3PO_4 photocatalysts synthesized from different phosphate salts (K_2HPO_4, KH_2PO_4, Na_2HPO_4, NaH_2PO_4) and (b) a position comparison of some FTIR peaks in the range of 400–1200 cm^{-1}.

Another useful tool for indirectly observing crystal structure and their small changes is the Raman scattering spectra (Figure 5). Figure 5a shows that in the range of wave number 200–1200 cm^{-1}, APO exhibits seven vibrational peaks centered at wave numbers of 151 cm^{-1}, 281 cm^{-1}, 406 cm^{-1}, 577 cm^{-1}, 910 cm^{-1}, 956 cm^{-1}, and 1057 cm^{-1}, all of them are characteristic vibrations of $[PO_4]$ cluster. The intensive peak at 910 cm^{-1} could be assigned to the symmetric stretching mode (A_1) of $[PO_4]$ group while the asymmetric stretching vibration (T_2) of this group are at 956 cm^{-1} and 1057 cm^{-1}. The peaks at 406 cm^{-1} and 577 cm^{-1} were the symmetric (E) and asymmetric (T_2) bending modes while the peaks at 151 cm^{-1} and 281 cm^{-1} were attributed to rotation or translation mode [34] of $[PO_4]$ unit. Figure 5b details the positions of several Raman peaks in the range of wave number 180–650 cm^{-1}, which shows a strong Raman shift in different samples. The two samples synthesized from dibasic salts exhibited vibration peaks at low wave numbers of about 239 cm^{-1}

and 557 cm^{-1} while these peaks are at 282 cm^{-1} and 582 cm^{-1} for the APOKH2 and APONaH2 samples. Theoretically, the vibration frequency is determined by the atomic mass and the interatomic spacing, thus the vibration frequency increase of [PO_4] cluster in APOKH2 and APONaH2 samples indirectly confirms the decrease of the lattice parameter, consistent well with XRD and FTIR results.

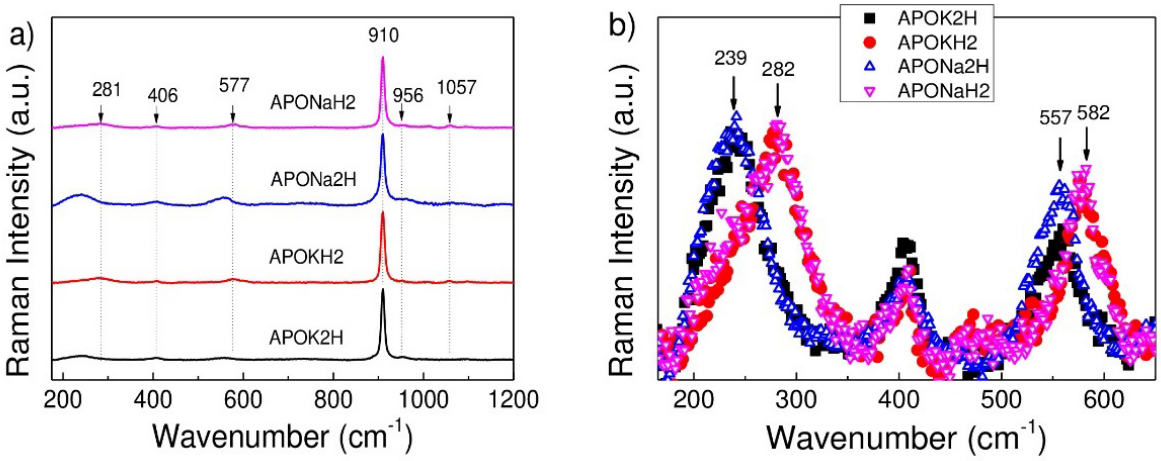

Figure 5. (a) Raman scattering spectra of Ag_3PO_4 photocatalysts synthesized from different phosphate salts (K_2HPO_4, KH_2PO_4, Na_2HPO_4, NaH_2PO_4) and (b) a position comparison of some Raman peaks in the range of 150–650 cm^{-1}.

Figure 6 shows UV-vis absorption spectra of APO synthesized from different phosphate salts (K_2HPO_4, KH_2PO_4, Na_2HPO_4, and NaH_2PO_4). All samples exhibit an absorption edge at around 530 nm, thus suitable for using part of visible light band for photocatalytic excitation. The absorption edge for two samples APOKH2 and APONaH2 shifts slightly to the larger wavelength comparing to that of APOK2H and APONa2H. The bandgap of the photocatalyst was determined by the Wood-Tauc plot method where $(\alpha h\nu)^2$ is graphed as a function of photon energy as for direct semiconductor (Figure 6b). The identified values of E_g are around of 2.38 eV and 2.42 eV for APOKH2/APONaH2 and APOK2H/APONa2H, respectively, which is in good agreement with previous studies [35,36]. This result shows that the samples APOKH2 and APONaH2 can even absorb a wider range of radiation in the visible range than the samples APOK2H and APONa2H. The correlation between band gap energy and crystal size is appropriately explained by the quantum size effect [37].

The photoluminescence PL spectra, which indirectly inform the recombination rate of photogenerated electron-hole, are shown in Figure 7. The result indicates that all samples emit irradiation over a wide range from 400 to 600 nm with a maximum between 500 to 530 nm and another at around 420 nm. PL properties of APO was attributed to the existence of [PO_4] and [AgO_4] clusters in which the blue PL emission is assumed to be caused by tetragonal [PO_4] unit while the distorted tetragonal [AgO_4] responds to the red PL emission [28,38]. Figure 7 shows that the different samples have slightly different PL intensities, where the APOK2H sample exhibits the lowest PL intensity, which can infer the smallest electron-hole recombination rate.

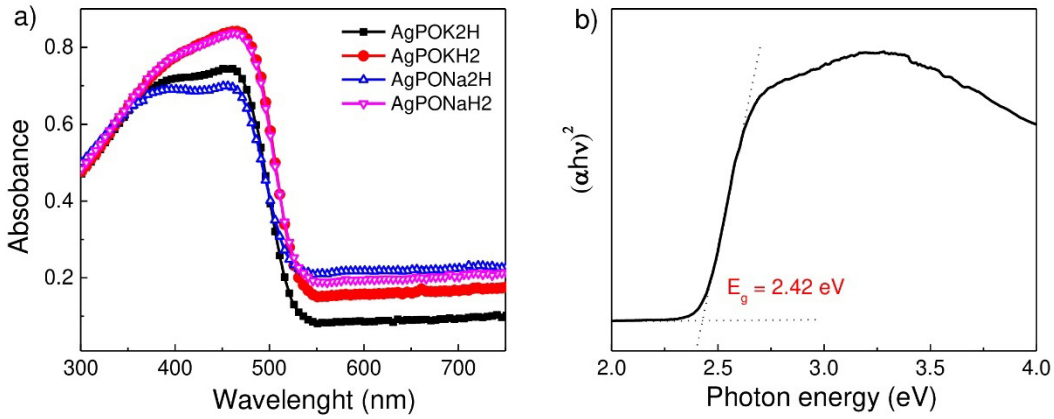

Figure 6. (a) UV-vis absorption spectra of as-synthesized Ag_3PO_4 with different starting phosphate salts and (b) the method to determine energy band gap from the plot of $(\alpha hv)^2$ versus photon energy (hc/λ).

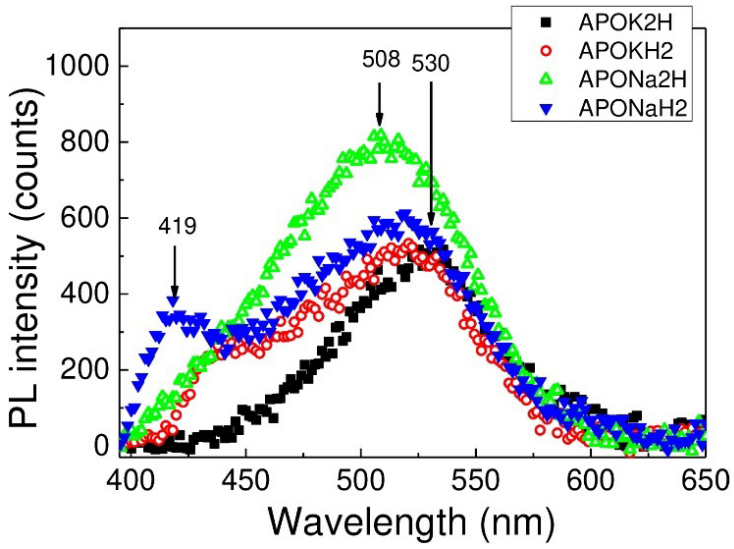

Figure 7. PL spectra of as-synthesized Ag_3PO_4 with different initial phosphate salts.

The photocatalytic properties of as-prepared APO were evaluated through the decomposition of RhB solution under the visible light irradiation. The remaining RhB concentrations at each time were assessed through the intensity of RhB characteristic absorption peak at 554 nm. Figure 8 shows the results of the photocatalytic test of the as-synthesized APO. During the first 30 min, the RhB solution was stirred in the dark to reach adsorption-desorption equilibrium. Figure 8a indicates that after only 10 min an equilibrium state was established. In addition, the adsorption capacity of APO photocatalysts is also very poor, only around 5%. This can be explained by the large particle size of the material (several μm) as observed. When illuminated, all samples showed high photocatalytic activity where APOK2H and APONa2H completely degraded RhB in just 8 min and 10 min while samples APOKH2 and APONaH2 required 20 and 25 min, respectively.

The photocatalytic reaction rate k was evaluated using the pseudo-first-order kinetic model, $ln(C_o/C) = kt$, where the reaction rate k could be obtained from the slope of the linear relationship of the plot $ln(C_o/C)$ versus reaction time (Figure 8b). The obtained values of k were 0.621, 0.444, 0.243, and 0.123 for APOK2H, APONa2H, APOKH2 and APONaH2, respectively. It is obvious that the visible light photocatalytic performance of APO samples synthesized from dibasic phosphate salts, which have poorer crystallinity and wider band gap, is better than that of the samples prepared from monobase salts. This can be attributed to the significant contribution of small particle size and therefore large specific surface area to the photocatalytic activity. However, APO prepared from potasium phosphate salts (monobasic or dibasic) is more active compared to APO synthesized from the salt of sodium, despite the larger particle size. This proves that in terms of selectivity, the phosphate salt of potassium is more suitable for the production of high photocatalytically active APO. The superior photocatalytic activity of APO is explained by the narrow bandgap energy. APO can effectively excited by visible light to produce electron-hole pairs that are directly involved in the oxidation of organic pollutants [39,40].

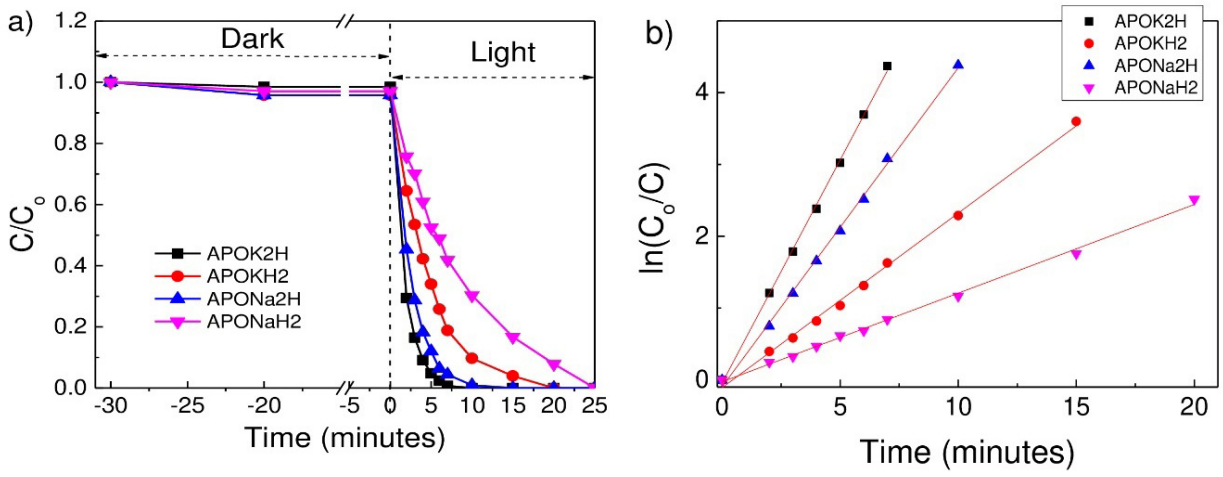

Figure 8. (a) Photocatalytic activities and (b) reaction rate of as-synthesized Ag_3PO_4 in decomposing RhB solution under visible light using Xenon lamp.

4. Conclusions

Dibasic and monobasic phosphate salts of potassium and sodium used as precipitants have a strong influence on the crystallinity, crystal size, optical properties and even the photocatalytic activity of Ag_3PO_4. When using dibasic phosphate salt, APO crystallizes slowly, leading to small particle size, low electron/hole recombination rate, and superior photocatalytic activity. In addition, APO also exhibits higher photocatalytic activity when prepared from phosphate salts of potassium metal.

Acknowledgements

This research was funded by a scientific and technological project at the level of Ministry of Education and Training, grand number B2020-MDA-11.

Conflict of interest

The authors declare that they have no conflict of interest.

Author contributions

Methodology and experiment, Mai Vu Thanh, Hang Lam Thi, Duyen Pham Thi, Dao La Bich, Anh Nguyen Thi Dieu; formal analysis, Hang Lam Thi, Duyen Pham Thi; investigation, Chung Pham Do, Hung Nguyen Manh; writing-original draft preparation, Oanh Le Thi Mai; writing-review and editing, Hung Nguyen Manh, Oanh Le Thi Mai, Chung Pahm Do; supervision, Minh Nguyen Van. All authors have read and agreed to the published version of the manuscript.

References

1. Asghar A, Abdul Raman AA, Wan Daud WMA (2015) Advanced oxidation processes for in-situ production of hydrogen peroxide/hydroxyl radical for textile wastewater treatment: a review. *J Clean Prod* 87: 826–838. https://doi.org/10.1016/j.jclepro.2014.09.010
2. Cuerda-Correa EM, Alexandre-Franco MF, Fernández-González C (2019) Advanced oxidation processes for the removal of antibiotics from water. An Overview. *Water* 12: 102. https://doi.org/10.3390/w12010102
3. Muruganandham M, Suri RPS, Jafari S, et al. (2014) Recent developments in homogeneous advanced oxidation processes for water and wastewater treatment. *Int J Photoenergy* 2014: 1–21. https://doi.org/10.1155/2014/821674
4. Fujishima A, Honda K (1972) Electrochemical photolysis of water at a semiconductor electrode. *Nature* 238: 37–38. https://doi.org/10.1038/238037a0
5. Khlyustova A, Sirotkin N, Kusova T, et al. (2020) Doped TiO_2: the effect of doping elements on photocatalytic activity. *Mater Adv* 1: 1193–1201. https://doi.org/10.1039/D0MA00171F
6. Ohno T, Akiyoshi M, Umebayashi T, et al. (2004) Preparation of S-doped TiO_2 photocatalysts and their photocatalytic activities under visible light. *Appl Cataly A-Gen* 265: 115–121. https://doi.org/10.1016/j.apcata.2004.01.007
7. Duan P, Han C, Zheng Y, et al. (2020) $A_2B_2O_7$ (A = La, Pr, Nd, Sm, Gd and B Ti, Zr, Sn) ceramics for mild-temperature NO_2 sensing and reduction. *J Alloy Compd* 831: 154866. https://doi.org/10.1016/j.jallcom.2020.154866
8. García-Ramírez E, Mondragón-Chaparro M, Zelaya-Angel O (2012) Band gap coupling in photocatalytic activity in ZnO–TiO_2 thin films. *Appl Phys A-Mater* 108: 291–297. https://doi.org/10.1007/s00339-012-6890-x

9. Reli M, Huo P, Sihor M, et al. (2016) Novel TiO_2/C_3N_4 photocatalysts for photocatalytic reduction of CO_2 and for photocatalytic decomposition of N_2O. *J Phys Chem A* 120: 8564–8573. https://doi.org/10.1021/acs.jpca.6b07236
10. Huo P, Tang Y, Zhou M, et al. (2016) Fabrication of $ZnWO_4$-CdS heterostructure photocatalysts for visible light induced degradation of ciprofloxacin antibiotic. *J Ind Eng Chem* 37: 340–346. https://doi.org/10.1016/j.cattod.2015.07.033
11. Ansari F, Sheibani S, Caudillo-Flores U, et al. (2020) Effect of TiO_2 nanoparticle loading by sol-gel method on the gas-phase photocatalytic activity of Cu_xO–TiO_2 nanocomposite. *J Sol-Gel Sci Techn* 96: 464–479. https://doi.org/10.1007/s10971-020-05388-8
12. Xing MY, Yang BX, Yu H, et al. (2013) Enhanced photocatalysis by Au nanoparticle loading on TiO_2 single-crystal (001) and (110) facets. *J Phys Chem Lett* 4: 3910–3917. https://doi.org/10.1021/jz4021102
13. George S, Pokhrel S, Ji Z, et al. (2011) Role of Fe doping in tuning the band gap of TiO_2 for the photo-oxidation-induced cytotoxicity paradigm. *J Am Chem Soc* 133: 11270–11278. https://doi.org/10.1021/ja202836s
14. Yi Z, Ye J, Kikugawa N, et al. (2010) An orthophosphate semiconductor with photooxidation properties under visible-light irradiation. *Nat Mater* 9: 559–564. https://doi.org/10.1038/nmat2780
15. Afifah K, Andreas R, Hermawan D, et al. (2019) Tuning the Morphology of Ag_3PO_4 Photocatalysts with an Elevated Concentration of KH_2PO_4. *Bull Chem React Eng* 14: 625–633. https://doi.org/10.9767/bcrec.14.3.4649.625-633
16. Sulaeman U, Permadi RD, Diastuti H (2021) The synthesis of Ag_3PO_4 under graphene oxide and hydroxyapatite aqueous dispersion for enhanced photocatalytic activity. *IOP Conf Ser-Earth Environ Sci* 746: 012040. http://dx.doi.org/10.1088/1755-1315/746/1/012040
17. Xu Y, Zhang X, Zhang Y, et al. (2020) Nano flake Ag_3PO_4 enhanced photocatalytic activity of bisphenol A under visible light irradiation. *Colloid Interfac Sci* 37: 100277. https://doi.org/10.1016/j.colcom.2020.100277
18. Zhang W, Zhang X, Dang X, et al. (2016) The role of graphene oxide in Ag_3PO_4/graphene oxide composites for enhanced visible-light-driven photocatalytic ability. *J Adv Oxid Technol* 19: 317–325. https://doi.org/10.1515/jaots-2016-0216
19. Zhang M, Du H, Ji J, et al. (2021) Highly efficient Ag_3PO_4/g-C_3N_4 Z-scheme photocatalyst for its enhanced photocatalytic performance in degradation of rhodamine B and phenol. *Molecules* 26: 2062. https://doi.org/10.3390/molecules26072062
20. Xu Z, Liu N, Wei Q, et al. (2021) Visible light-driven Ag_3PO_4@resin core-shell microspheres for photocatalytic degradation of methylene blue. *Chem Phys Lett* 772: 138591.
21. Tab A, Dahmane M, Chemseddin B, et al. (2020) Photocatalytic degradation of quinoline yellow over Ag_3PO_4. *Catalysts* 10: 138591. https://doi.org/10.1016/j.cplett.2021.138591
22. Osman NS, Sulaiman SN, Muhamad EN, et al. (2021) Synthesis of an Ag_3PO_4/Nb_2O_5 photocatalyst for the degradation of dye. *Catalysts* 11: 458. https://doi.org/10.3390/catal11040458

23. Wang X, Utsumi M, Yang Y, et al. (2013) Removal of microcystins (-LR, -YR, -RR) by highly efficient photocatalyst Ag/Ag_3PO_4 under simulated solar light condition. *Chem Eng J* 230: 172–179. http://dx.doi.org/10.1016/j.cej.2019.123765
24. Dong P, Yin Y, Xu N, et al. (2014) Facile synthesis of tetrahedral Ag_3PO_4 mesocrystals and its enhanced photocatalytic activity. *Mater Res Bull* 60: 682–689. https://doi.org/10.1016/j.materresbull.2014.09.047
25. Batvandi M, Haghighatzadeh A, Mazinani B (2020) Synthesis of Ag_3PO_4 microstructures with morphology-dependent optical and photocatalytic behaviors. *Appl Phys A-Mater* 126: 571. https://link.springer.com/article/10.1007/s00339-020-03761-6
26. Febiyanto F, Soleh A, Amal MSK, et al. (2019) Facile synthesis of Ag_3PO_4 photocatalyst with varied ammonia concentration and its photocatalytic activities for dye removal. *Bull Chem ReactEng* 14: 42–50. https://doi.org/10.9767/bcrec.14.1.2549.42-50
27. Deng P, Xiong J, Lei S, et al. (2019) Nickel formate induced high-level in situ Ni-doping of g-C_3N_4 for a tunable band structure and enhanced photocatalytic performance. *J Mater Chem A* 7: 22385–22397. http://dx.doi.org/10.1039/C9TA04559G
28. Botelho G, Andres J, Gracia L, et al. (2016) Photoluminescence and photocatalytic properties of Ag_3PO_4 microcrystals: An experimental and theoretical investigation. *Chempluschem* 81: 202–212. https://doi.org/10.1002/cplu.201500485
29. Amornpitoksuk P, Intarasuwan K, Suwanboon S, et al. (2013) Effect of phosphate salts (Na_3PO_4, Na_2HPO_4, and NaH_2PO_4) on Ag_3PO_4 morphology for photocatalytic dye degradation under visible light and toxicity of the degraded dye product. *Ind Eng Chem Res* 52: 17369–17375. http://dx.doi.org/10.1021/ie401821w
30. Futihah I, Riapanitra A, Yin S, et al. (2020) The pH dependence of Ag_3PO_4 synthesis on visible light photocatalytic activities. *J Phys-Conf Ser* 1494: 012027. http://dx.doi.org/10.1088/1742-6596/1494/1/012027
31. Aufort J, Lebon M, Gallet X, et al. (2018) Macroscopic electrostatic effects in ATR-FTIR spectra of modern and archeological bones. *Am Mineral* 103: 326–329. https://doi.org/10.2138/am-2018-6320CCBYNCND
32. Destainville A, Champion E, Bernache-Assollant D, et al. (2003) Synthesis, characterization and thermal behavior of apatitic tricalcium phosphate. *Mater Chem Phys* 80: 269–277. https://doi.org/10.1016/S0254-0584(02)00466-2
33. Infrared Spectroscopy, Chemistry LibreTexts, 2022. Available from: https://chem.libretexts.org/@go/page/1847.
34. Trench AB, Machado TR, Gouveia AF, et al. (2018) Connecting structural, optical, and electronic properties and photocatalytic activity of Ag_3PO_4:Mo complemented by DFT calculations. *Appl Catal B-Environ* 238: 198–211. https://doi.org/10.1016/j.apcatb.2018.07.019
35. Song L, Yang J, Zhang S (2017) Enhanced photocatalytic activity of Ag_3PO_4 photocatalyst via glucose-based carbonsphere modification. *Chem Eng J* 309: 222–229. https://doi.org/10.1016/j.cej.2016.10.035
36. Liu Y, Qian Q, Yi Z, et al. (2013) Low-temperature synthesis of single-crystalline $BiFeO_3$ using molten KCl–KBr salt. *Ceram Int* 39: 8513–8516. https://doi.org/10.1016/j.ceramint.2013.03.025

37. Marotti RE, Giorgi P, Machado G, et al. (2006) Crystallite size dependence of band gap energy for electrodeposited ZnO grown at different temperatures. *Solar Energ Mat Sol C* 90: 2356–2361. https://doi.org/10.1016/j.solmat.2006.03.008
38. Botelho G, Sczancoski JC, Andres J, et al. (2015) Experimental and theoretical study on the structure, optical properties, and growth of metallic silver nanostructures in Ag_3PO_4. *J Phys Chem C* 119: 6293–6306. http://dx.doi.org/10.1021/jp512111v
39. Zheng F, Wu D, Xia J, et al. (2015) Visible light photocatalytic degradation of Methyl orange by Ag_3PO_4/TiO_2 coated self-cleaning cotton. *J Optoelectron Adv M* 17: 1528–1531.
40. Hsieh MS, Su HJ, Hsieh PL, et al. (2017) Synthesis of Ag_3PO_4 crystals with tunable shapes for facet-dependent optical property, photocatalytic activity, and electrical conductivity Examinations. *ACS Appl Mater Interfaces* 9: 39086–39093. https://doi.org/10.1021/acsami.7b13941

AIMS Press